Planar Solid-State and Solution Structures of (Porphinato)nickel(II) As Determined by X-ray Diffraction and Resonance Raman Spectroscopy

Walter Jentzen,*,† Ilona Turowska-Tyrk,‡ W. Robert Scheidt,*,‡ and John A. Shelnutt*,†,§

Fuel Science Department, Sandia National Laboratories, Albuquerque, New Mexico 87185-0710, Department of Chemistry and Biochemistry, University of Notre Dame, Notre Dame, Indiana 46556, and Department of Chemistry, University of New Mexico, Albuquerque, New Mexico 87131

Received February 9, 1996[⊗]

The structure of (porphinato)nickel(II) [Ni(P)] has been determined by X-ray diffraction and inferred from a combination of single-crystal and solution resonance Raman measurements. The crystal structure reveals a planar porphyrin macrocycle with a $\pi-\pi$ dimer packing configuration exhibiting a small lateral shift. This group S crystallographic packing arrangement has been suggested to give strong $\pi-\pi$ interactions between the porphyrin rings on the basis of the small interplanar spacing (3.355 Å) and lateral shift (1.528 Å) between the porphine planes. Strong $\pi-\pi$ interactions are usually associated with geometrically inequivalent structural parameters such as different metal−nitrogen bond distances, but this is not observed for Ni(P). The average nickel−nitrogen bond distance is 1.951 Å, consistent with planar nickel porphyrins. The root-mean-square out-of-plane displacement from the mean plane of the macrocyclic atoms is 0.019 Å, consonant with the observed very slight ruffling of the macrocycle. A salient feature of the resonance Raman spectra of Ni(P) in solution is the apparent sidebands of some structure-sensitive lines. This observation was interpreted previously as resulting from an equilibrium between planar and nonplanar conformers in solution. However, the similarities of the resonance Raman spectra of Ni(P) in the single crystal and in solution suggest that Ni(P) exists only in the planar conformation. This conclusion is corroborated by solution resonance Raman spectra of the four-coordinate (porphinato)copper(II) and (porphinato)-cobalt(II), which are more likely than Ni(P) to be planar because of their larger central metals, yet they also show the sidebands of the same structure-sensitive lines. Crystal data: $[C_{20}H_{12}N_4]Ni$; $a = 10.1066(7)$ Å, $b = 11.945(9)$ Å, $c = 12.229(2)$ Å, $\beta = 101.56(3)°$, $Z = 4$, $V = 1446.4(11)$ Å^3, space group $P2_1/c$; 3084 unique observed data; refinement converged to final values of $R_1 = 0.039$, w$R_2 = 0.090$; all measurements at 127(2) K.

Introduction

Metalloporphyrins are of importance because of their substantial role in biological systems such as the photosynthetic reaction centers,[1] methylreductase,[2] vitamin B_{12},[3] cytochromes,[4,5] and heme proteins,[6,7] to name only a few. Nonplanar porphyrins and their conformational changes are of great interest as a possible mechanism for protein modulation of the biological properties of tetrapyrroles. Nonplanar distortions may influence basic properties like redox potential,[8−10] axial ligation,[8] electron-transfer rate,[8,11] and photophysical processes.[12−15] For instance, theoretical calculations and experimental results have shown that the relative energy gap between the highest occupied (HOMO) and lowest unoccupied molecular orbitals (LUMO) is strongly affected by nonplanar distortions altering their light absorption properties and reduction potentials. One case in which this might be important is for the *c*-type cytochromes. The nonplanar distortion of the heme group is a result of covalent binding to the protein,[5] nonbonding interactions with the amino acid groups,[5,7,8,11] and axial ligand binding.[6c,17] Similar nonplanar structures in synthetic metalloporphyrins can be modeled by introducing bulky substituents at the porphyrin periphery,[13−16] incorporating small central metal ions,[16b,18] and binding of axial ligands.[17,19]

* Authors to whom correspondence should be addressed.
† Sandia National Laboratories.
‡ University of Note Dame.
§ University of New Mexico.
⊗ Abstract published in *Advance ACS Abstracts,* May 15, 1996.

(1) (a) Deisenhofer, J.; Epp, O.; Miki, K.; Huber, R.; Michel, H. *J. Mol. Biol*. **1984**, *180*, 385. (b) Deisenhofer, J.; Epp, O.; Miki, K.; Huber, R.; Michel, H. *Nature*. **1985**, *318*, 618. (c) Zinth, W.; Knapp, E. W.; Fischer, S. F.; Kaiser, W.; Deisenhofer, J.; Michel, H. *Chem. Phys. Lett*. **1985**, *119*, 1. (d) Deisenhofer, J.; Michel, H. *Science*. **1989**, *245*, 1463.
(2) (a) Furenlid, L. R.; Renner, M. W.; Fajer, J. *J. Am. Chem. Soc*. **1990**, *112*, 8987. (b) Furenlid, L. R.; Renner, M. W.; Smith, K. M.; Fajer, J. *J. Am. Chem. Soc*. **1990**, *112*, 1634.
(3) Geno, M. K.; Halpern, J. *J. Am. Chem. Soc*. **1987**, *109*, 1238.
(4) Moore, G. R.; Pettigrew, G. W. *Cytochromes c: Evolutionary, Structural, Physicochemical Aspects*; Springer-Verlag: Berlin, 1990.
(5) Hobbs, J. D.; Shelnutt, J. A. *J. Protein Chem*. **1995**, *14*, 19.
(6) (a) Hoard, J. L. In *Hemes and Heme Proteins*; Chance, B., Estabrock, R. W., Yontenani, T., Eds.; Academic Press: New York, 1966. (b) Antonini, E.; Brunori, M. *Hemoglobin and Myoglobin in their Reactions with Ligands*; North Holland Publishing Co. Amsterdam, 1971. (c) Baldwin, J. L.; Chothia, C. *J. Mol. Biol*. **1979**, *129*, 175.
(7) Alden, R. G.; Ondrias, M. R.; Shelnutt, J. A. *J. Am. Chem. Soc*. **1990**, *112*, 691.
(8) Barkigia, K. M.; Chantranupong, L.; Smith, K. M.; Fajer, J. *J. Am. Chem. Soc*. **1988**, *110*, 7566.
(9) (a) Kadish, K. M.; Van Caemelbecke, E.; D'Souza, F. D.; Medforth, C. J.; Smith, K. M.; Tabard, A. *Organometallics* **1993**, *12*, 2411. (b) Kadish, K. M.; Van Caemelbecke, E.; Boulas, P.; D'Souza, F. D.; Vogel, E.; Kisters, M.; Medforth, C. J.; Smith, K. M. *Inorg. Chem*. **1993**, *32*, 4177.
(10) (a) Kratky, C.; Waditschatka, R.; Angst, C.; Johansen, J.; Plaquevent, J. C.; Schreiber, J.; Eschenmoser, A. *Helv. Chim. Acta* **1982**, *68*, 1312. (b) Waditschatka, R.; Kratky, C.; Jaun, B.; Heinzer, J.; Eshenmoser, A. *J. Chem. Soc., Chem. Commun*. **1985**, 1604.
(11) Plato, M.; Mobius, K.; Michel-Beyerle, M. E.; Bixon, M.; Jortner, J. *J. Am. Chem. Soc*. **1988**, *110*, 7279.
(12) Gudowska-Nowak, E.; Newton, M. D.; Fajer, J. *J. Phys. Chem*. **1990**, *94*, 5795.
(13) Medforth, C.J.; Berber, M. D.; Smith, K. M.; Shelnutt, J. A. *Tetrahedron Lett*. **1990**, *31*, 3719.
(14) Shelnutt, J. A.; Medforth, C. J.; Berber, M. D.; Barkigia, K. M.; Smith, K. M. *J. Am. Chem. Soc*. **1991**, *113*, 4077.
(15) Jentzen, W.; Simpson, M. C.; Hobbs, J. D.; Song, X.; Ema, T.; Nelson, N. Y.; Medforth, C. J.; Smith, K. M.; Veyrat, M.; Mazzanti, M.; Ramasseul, R.; Marchon, J.-C.; Takeuchi, T.; Goddard, W. A., III; Shelnutt, J. A. *J. Am. Chem. Soc*. **1995**, *117*, 11085.

S0020-1669(96)00157-7 CCC: $12.00

The ultimate goal in using synthetic metalloporphyrins as model compounds for porphyrin−protein interactions is to gain an understanding of the relationships between the structure and function of the naturally occurring porphyrins. The degree of nonplanarity of metalloporphyrins primarily depends on the size of the central metal and the size, shape, and orientation of the substituents.[13−18] Small metals like nickel(II) favor nonplanar distortions like ruffling and saddling which allow shorter metal−nitrogen distances. Bulky substituents also result in these and other nonplanar conformations that relieve steric crowding at the periphery of the macrocycle. Clearly, highly nonplanar metalloporphyrins are favored for tetrapyrroles having small central metals and bulky substituents as, for example, (2,3,7,8,-12,13,17,18-octaethyl-5,10,15,20-tetraphenylporphinato)nickel-(II).[20] On the other hand, more planar macrocycles are observed for metalloporphyrins with less bulky substituents and central metals like copper(II) and zinc(II) which give core sizes closer to the optimum porphyrin core of about 2.00 Å [*e.g.*, (2,3,7,8,-12,13,17,18-octaethylporphinato)copper(II)[21]].

An intermediate case, however, exists for porphyrins with small metals and also relatively few and small substituents. For many of these metalloporphyrins, an equilibrium between planar and nonplanar structures is found in solution. For instance, Ni-(OEP) [(2,3,7,8,12,13,17,18-octaethylporphinato)nickel(II)] crystallizes in two planar triclinic *A* and *B* forms[22,23] and a nonplanar tetragonal form.[24] These different structures can be distinguished spectroscopically in that they give rise to different frequencies for the structure-sensitive Raman lines ν_3, ν_{11}, ν_2, ν_{19}, and ν_{10}.[25] In solution, the Raman spectrum of Ni(OEP) shows that most of these structure-sensitive lines are clearly asymmetric and can be described well by two sublines attributed to equilibrium between planar and nonplanar conformers mainly on the basis of a comparison with single-crystal and solution Raman spectra.[26]

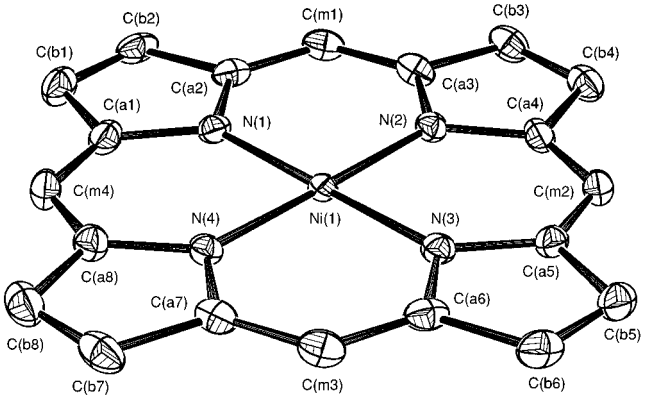

Figure 1. ORTEP[30b] diagram of Ni(P) giving the crystallographic atom-labeling scheme. Atoms are contoured at the 50% probability level (hydrogen atoms are not shown). The three distinguishable carbons C(a), C(b), and C(m) (notation used in crystallography) with respect to their positions are usually denoted in vibrational spectroscopy by the symbols C_α, C_β, and C_m, respectively. In this work, the later notation is used in the text.

With only hydrogens at the porphyrin periphery, metalloporphyrins are the simplest, least sterically crowded metalloporphyrins (Figure 1). Thus, they would be expected to tend toward planarity even for small metals like nickel(II). However, there is a paucity of structural information for metalloporphines in part because of their poor solubility. The present work is intended to give more structural and spectroscopic information about metalloporphines, especially with respect to the effect of reduced steric interactions at the porphyrin periphery.

X-ray diffraction and resonance Raman spectroscopy are useful methods for investigating the structures of porphyrins. Furthermore, both methods reveal important information pertaining to porphyrin−porphyrin interactions such as $\pi-\pi$ interactions. For example, the above structure-sensitive Raman lines shift their frequency positions for different crystal packing arrangements[19,21b,23] or aggregation in solution[7,27] as a result of changes in the π charge density in the porphyrin rings.

Herein, the X-ray crystal structure and the single-crystal and solution resonance Raman spectra of Ni(P) are reported and used to obtain its solid-state and solution structures. The X-ray crystal structure of Ni(P) clearly exhibits a planar macrocycle in a small laterally shifted dimer configuration. Because of this crystal packing arrangement, the Ni(P) molecules are expected to interact strongly via $\pi-\pi$ interactions. However, unexpectedly small frequency differences between the solid state and solution for the structure-sensitive lines are found. Furthermore, the sidebands of some structure-sensitive Raman lines, which were previously interpreted in terms of an equilibrium between two conformers in solution,[28,29] are also observed in the single-crystal spectra. This convincingly shows that Ni(P) exhibits only a planar structure in solution. A possible origin of the sidebands of the structure-sensitive Raman lines is proposed.

Materials and Methods

Materials. The metalloporphines Ni(P), Cu(P), and Co(P) were purchased from Porphyrin Products and were purified by liquid column chromatography using carbon disulfide (CS_2) as the mobile phase

(16) (a) Medforth, C. J.; Senge, M. O.; Smith, K. M.; Sparks, L. D.; Shelnutt, J. A. *J. Am. Chem. Soc.* **1992**, *114*, 9859. (b) Shelnutt, J. A.; Majumder, S. A.; Sparks, L. D.; Hobbs, J. D.; Medforth, C. J.; Senge, M. O.; Smith, K. M.; Miura, M.; Quirke, J. M. E. *J. Raman Spectrosc.* **1992**, *23*, 523. (c) Hobbs, J. D.; Majumder, S. A.; Luo, L.; Sickelsmith, G. A.; Quirke, J. M. E.; Medforth, C. J.; Smith, K. M.; Shelnutt, J. A. *J. Am. Chem. Soc.* **1994**, *116*, 3261. (d) Miura, M.; Majumder, S. A.; Hobbs, J. D.; Renner, M. W.; Furenlid, L. R.; Shelnutt, J. A. *J. Am. Chem. Soc.* **1994**, *33*, 6078.
(17) Medforth, C. J.; Muzzi, C. M.; Shea, K. M.; Smith, K. M.; Abraham, R. J.; Jia, S.; Shelnutt, J. A. Submitted for publication.
(18) (a) Sparks, L. D.; Medforth, C. J.; Park, M.-S.; Chamberlain, J. R.; Ondrias, M. R.; Senge, M. O.; Smith, K. M.; Shelnutt, J. A. *J. Am. Chem. Soc.* **1993**, *115*, 581. (b) Sparks, L. D.; Anderson, K. K.; Medforth, C. J.; Smith, K. M.; Shelnutt, J. A. *Inorg. Chem.* **1994**, *33*, 2297.
(19) Scheidt, W. R.; Lee, Y. J. *Struct. Bonding (Berlin)* **1987**, *64*, 1.
(20) Renner, M. W.; Barkigia, K. M.; Zhang, Y.; Medforth, C. J.; Smith, K. M.; Fajer, J. *J. Am. Chem. Soc.* **1994**, *116*, 8582.
(21) (a) Pak, R.; Scheidt, W. R. *Acta Crystallogr., Sect. C* **1991**, *47*, 431. (b) Sparks, L. D.; Scheidt, W. R.; Shelnutt, J. A. *Inorg. Chem.* **1992**, *31*, 2191.
(22) Cullen, D. L.; Meyer, E. F. *J. Am. Chem. Soc.* **1974**, *96*, 2095.
(23) Brennan, T. D.; Scheidt, W. R.; Shelnutt, J. A. *J. Am. Chem. Soc.* **1988**, *110*, 3919.
(24) Meyer, E. F. *Acta Crystallogr., Sect. B* **1972**, *28*, 2162.
(25) Czernuszewicz, R. S.; Li, X.-Y.; Spiro, T. G. *J. Am. Chem. Soc.* **1989**, *111*, 7024.
(26) (a) Alden, R. G.; Crawford, B. A.; Doolen, R.; Ondrias, M. R.; Shelnutt, J. A. *J. Am. Chem. Soc.* **1989**, *111*, 2070. (b) Anderson, K. K.; Hobbs, J. D.; Luo, L.; Stanley, K. D.; Quirke, J. M. E.; Shelnutt, J. A. *J. Am. Chem. Soc.* **1993**, *115*, 12346. (c) Jentzen, W.; Dreybrodt, W.; Schweitzer-Stenner, R. *Biophys. J.* **1993**, *64*, A155. (d) Jentzen, W.; Schweitzer-Stenner, R.; Dreybrodt, W. In *Proceedings of the Fifth International Conference on the Spectroscopy of Biological Systems*; Theophanides, T., Anastassopoulou, J., Fotopoulos, N., Eds.; Kluwer Academic Publishers: Dordrecht, The Netherlands, 1993; p 33. (e) Jentzen, W.; Unger, E.; Karvounis, G.; Shelnutt, J. A.; Dreybrodt, W.; Schweitzer-Stenner, R. Submitted for publication.
(27) (a) Shelnutt, J. A.; Dobry, M. M. *J. Phys. Chem.* **1983**, *87*, 3012. (b) Satterlee, J. D.; Shelnutt, J. A. *J. Phys. Chem.* **1984**, *88*, 5487. (c) Shelnutt, J. A.; Dobry, M. M.; Satterlee, J. D. *J. Phys. Chem.* **1984**, *88*, 4980. (d) Satterlee, J. D.; Shelnutt, J. A. *Inorg. Chim. Acta* **1985**, *106*, 165.
(28) Unger, E.; Bobinger, U.; Dreybrodt, W.; Schweitzer-Stenner, R. *J. Phys. Chem.* **1993**, *97*, 9956.
(29) Jentzen, W. Ph.D. Thesis, University of Bremen, Germany, Jan 1994.

(column 1 × 10 cm^2; Silica 32−63, 60 A, ICN Biomedicals). The integrity of the samples was monitored by thin-layer chromatography using Kieselgel with the fluorescence indicator F254 (Merck) and CS_2 as solvent. All solvents used were HPLC grade (Aldrich). The single crystal of Ni(P) was grown by very slow evaporation from CS_2 solution. After 5 months, one large black plate-shaped crystal was obtained. This large crystal was cleaved and used for X-ray diffraction to yield a specimen with dimensions of 30 × 330 × 400 μm^3.

X-ray Diffraction. The crystal of Ni(P) was examined with graphite-monochromated Mo Kα radiation on an Enraf-Nonius FAST[30a] area detector diffractometer at 127 K. Unit cell parameter determinations and data collection procedures are described elsewhere.[31] A total of 10 241 reflections were collected and averaged. Of these, 3693 were unique, and intensities of 3084 unique reflections were greater than $2\sigma(I)$. All reflections were reduced using Lorentz−polarization and absorption corrections.[32] The structure was solved by Patterson methods from the SHELXS-86 program[33]—all atoms were clearly seen in an *E* map. All non-hydrogen atoms of the structure were refined isotropically and afterward anisotropically by the use of SHELXL-93.[34] Hydrogen atoms were clearly seen in a difference Fourier map but were included as fixed, idealized contributors. The refinement converged to final values of $R_1 = 0.039$ and $wR_2 = 0.090$ for the observed unique reflections [$I > 2\sigma(I)$] and $R_1 = 0.052$ and $wR_2 = 0.096$ for all unique reflections, including negative intensities (the weighted *R* index is based on F^2). The maximum and minimum electron densities on the final difference Fourier map were 0.4 and −0.74 e/$Å^3$, respectively.

Spectroscopy. Raman spectra were obtained by using dual-channel spectroscopy.[35] Krypton and argon ion lasers (both Coherent, Innova 20) provided excitation wavelengths in the B(Soret)- and Q-band regions of the absorption spectrum. Interference filters were used to suppress the interfering plasma lines of the gas ion lasers. A collection lens with a 30-cm focal length focused the laser beam onto the sample. The scattered light was collected in a 90° scattering geometry by using a camera objective (Canon lens 50 mm, 1:0.95; effective *f*/1.4) and imaged onto the entrance slit of a spectrometer equipped with a cooled photomultiplier (Hamamatsu, type R928P) and photon-counting electronics (Tennelec, TC532 and TC593; LRS 133B and 123; Colorado Data System, 63B IAC System). Polarized spectra were measured by passing the scattered light through a Polaroid sheet oriented parallel or perpendicular to the scattering plane followed by a scrambler in front of the spectrometer entrance slit.

The solution Raman spectra and the corresponding reference spectra for frequency calibration were obtained simultaneously. The solution spectra of porphine samples and reference (benzene) were obtained by using a cylindrical rotating quartz cell consisting of two separate compartments. Rotation of the Raman cell at 50 Hz and low porphine concentration (less than 0.1 mM) prevented local heating of the sample even with incident laser powers as high as 100 mW. The single crystal of Ni(P) was placed between two thin quartz slides. The spectra were detected by mounting the sample holder and the reference (pencil lamps) in front of the camera objective, and the single-channel detection mode was used. In contrast to the technique used to obtain the solution spectra, the collection lens, which focused the laser beam onto the crystal, was defocused and the laser power was less than 20 mW to avoid strong local heating of the single crystal. After several scans, no sample decomposition was observed upon checking the sample integrity of the single crystal under the microscope and upon comparing the signals before and after the Raman measurements. The spectra shown in the figures are the unsmoothed sums of several scans; the detailed conditions are described in the figure captions.

Frequency calibrations were carried out by using benzene lines for the solution spectra, whereas the single-crystal spectra were calibrated with the spectral lines of the argon or krypton pencil lamps (Oriel). The observed peak positions of the benzene lines[29,36] used were taken to be 606.7, 992.2, and 1586.4/1606.2 cm^{-1} (Fermi doublet) which also serve as frequency standards for the pencil lamps. In addition, all spectra were corrected for nonlinearity of the spectrometer to obtain the absolute frequency positions of the lines. The reproducibility of the spectra were verified by recording the spectra several times. The peak positions and (true) line widths (full width at half-maximum) were obtained by decomposing the spectra into Lorentzian lines convoluted with a triangularly shaped spectral slit function of the spectrometer (*vide infra*).[37] The nonlinear least-squares curve-fitting was carried out with the program PeakFit (Jandel Scientific). The standard deviation in the absolute frequency reading was ±0.6 cm^{-1} for solution and ±1.0 cm^{-1} for single-crystal spectra unless otherwise explicitly stated.

Finally, the spectral slit width $\tilde{s}$ (full width at half-maximum) of the spectrometer used (Spex 1401, Czerny−Turner double monochromator) was calculated by employing the following equation:[29]

$$\tilde{s} = \frac{S\tilde{\nu}d}{4mf}\sqrt{4\tilde{\nu}^2 - (m/d)^2}$$

S is the geometrical entrance (and exit) slit width, $\tilde{\nu}$ the absolute wavenumber position, *f* the collimator focal length of the spectrometer, *d* the spacing of the grating, and *m* the diffraction order. The spectrometer used has $d = 1/1200$ mm, $m = 1$, and $f = 850$ mm which for $S = 100$ μm and $\lambda = 1/\tilde{\nu} = 413$ nm (at the Rayleigh line position of the excitation wavelength) gives a spectral slit width of $\tilde{s} = 2.8$ cm^{-1}. The experimentally determined slit function via spectral lines of krypton and argon pencil lamps can be described rather well with a triangular slit function for $S > 80$ μm. The maximum deviations of the experimentally determined spectral slit widths from the calculated ones were less than 8%.

The absorption spectra were measured by using a Hewlett-Packard 8452 A diode array spectrophotometer and 10-mm quartz cell. The porphine concentrations in solution were estimated from the maximum absorbance of the B band. The extinction coefficients ϵ for Ni(P), Cu(P), and Co(P) in CS_2 and CH_2Cl_2 were not available, so that the published extinction coefficients of the corresponding metal octaethylporphyrins (OEP) were used to estimate the porphine sample concentrations. The B-band extinction coefficients λ_{peak}/nm (ϵ_{peak}/mM^{-1} cm^{-1}) are for Ni(OEP) in CS_2 406 (170),[29] Cu(OEP) in CS_2 412 (273),[38a] and Co(OEP) in benzene 394 (229).[38b] On the basis of these extinction coefficients, the accuracy of the porphine concentration is 10%.

Results

X-ray Diffraction. Ni(P) is planar in the X-ray crystal structure. Figure 1 displays the molecular crystal structure along with the crystallographic atom-labeling scheme used. A summary of the crystallographic data is given in Table 1, and the final fractional atomic coordinates are listed in Table 2. (The hydrogen fractional atomic coordinates are given in Table S1

(30) (a) FAST is an acronym for fast-scanning area sensitive television detector. (b) ORTEP is an acronym for Oak Ridge thermal ellipsoid program.
(31) Scheidt, W. R.; Turowska-Tyrk, I. *Inorg. Chem.* **1994**, *33*, 1314.
(32) The process is based on an adaption of the DIFABS logic (Walker, N. P. *Acta Crystallogr., Sect. A* **1983**, *39*, 158) to area detector geometry by Karaulov (Karaulov, A. I. Personal communication, School of Chemistry and Applied Chemistry, University of Wales, College of Cardiff, Cardiff CF1 3TB, U.K.).
(33) Sheldrick, G. M. *Acta Crystallogr., Sect. A* **1990**, *46*, 467.
(34) Programs used in this study included SHELXL-93 (Sheldrick, G. M. *J. Appl. Crystallogr.*, in press) and ORTEP (Johnson, C. K. *ORTEP: A Fortran Thermal-Ellipsoid Plot Program For Crystal Structure Illustrations*; Oak Ridge National Laboratory: Oak Ridge, TN, 1970). Scattering factors were taken from Wilson, A.J.C. *International Tables of Crystallography*; Kluwer Academic Publishers: Dordrecht, The Netherlands, 1992; Vol. C.
(35) Shelnutt, J. A. *J. Phys. Chem.* **1983**, *87*, 605.
(36) Varchmin, J. Ph.D. Thesis, Ludwig-Maximilians-University, Munich, Germany, May 1967.
(37) (a) Torkington, P. *Appl. Spectrosc.* **1980**, *34*, 189. (b) Arora, A. K.; Umadevi, V. *Appl. Spectrosc.* **1982**, *36*, 424.
(38) (a) The extinction coefficients in CS_2 are based on the extinction coefficients of Cu(OEP) in dioxane taken from Somaya (Somaya, O. Ph.D. Thesis, University of Braunschweig, Germany, Dec 1967). Jentzen, W. Unpublished reseults. (b) Fuhrhop, J. H.; Smith, K. M. *Laboratory methods in porphyrin and metalloporphyrin research*; Elsevier Scientific Publishing: Amsterdam, 1977.

Table 1. Crystallographic Data for (Porphinato)nickel(II) [Ni(P)][a]

formula	$[C_{20}H_{12}N_4]Ni$	a/Å	10.1066(7)
fw	367.05	b/Å	11.945(9)
space group	$P2_1/c$	c/Å	12.229(2)
λ/Å	0.710 73	β/deg	101.56(3)
T/K	127(2)	R_1[b]	0.039
ρ/g cm^{-3}	1.686	wR_2[b]	0.090
μ/mm^{-1}	1.35	R_1[c]	0.052
crystal system	monoclinic	wR_2[c]	0.096
V/Å^{-3}	1446.4(11)	goodness-of-fit[d]	1.08
Z	4		

[a] Estimated standard deviations are given in parentheses. [b] Final R indices are based on $I > 2\sigma(I)$. $R = \sum||F_o| - |F_c||/\sum|F_o|$ and w$R = [\sum w(|F_o| - |F_c|)^2/\sum wF_o^2]^{1/2}$. [c] R indices for all data. [d] Goodness-of-fit based on F^2.

Table 2. Fractional Atomic Coordinates and Equivalent Isotropic Displacement Parameters (Å^2) for (Porphinato)nickel(II) [Ni(P)][a]

atom	x	y	z	U(eq)[b]
Ni(1)	0.03372(3)	0.12528(3)	0.08975(2)	0.01310(9)
N(1)	0.1711(2)	0.2260(2)	0.05401(14)	0.0161(4)
N(2)	0.1747(2)	0.0332(2)	0.17849(14)	0.0160(4)
N(3)	−0.1034(2)	0.0252(2)	0.12653(14)	0.0161(4)
N(4)	−0.1071(2)	0.2193(2)	0.00279(14)	0.0163(4)
C(a1)	0.1519(3)	0.3209(2)	−0.0111(2)	0.0207(5)
C(a2)	0.3093(2)	0.2181(2)	0.0885(2)	0.0191(4)
C(a3)	0.3125(2)	0.0500(2)	0.1987(2)	0.0202(5)
C(a4)	0.1593(3)	−0.0647(2)	0.2344(2)	0.0195(5)
C(a5)	−0.0843(3)	−0.0712(2)	0.1897(2)	0.0191(5)
C(a6)	−0.2415(5)	0.0345(2)	0.0938(2)	0.0199(5)
C(a7)	−0.2447(2)	0.2035(2)	−0.0153(2)	0.0198(5)
C(a8)	−0.0920(3)	0.3158(2)	−0.0559(2)	0.0211(5)
C(b1)	0.2783(3)	0.3719(2)	−0.0178(2)	0.0255(5)
C(b2)	0.3753(3)	0.3084(2)	0.0436(2)	0.0239(5)
C(b3)	0.3828(3)	−0.0371(2)	0.2673(2)	0.0239(5)
C(b4)	0.2879(3)	−0.1086(2)	0.2890(2)	0.0233(5)
C(b5)	−0.2107(3)	−0.1219(2)	0.1966(2)	0.0239(5)
C(b6)	−0.3083(3)	−0.0565(2)	0.1379(2)	0.0241(5)
C(b7)	−0.3153(3)	0.2905(2)	−0.0853(2)	0.0254(5)
C(b8)	−0.2202(3)	0.3600(2)	−0.1100(2)	0.0265(5)
C(m1)	0.3763(2)	0.1371(2)	0.1575(2)	0.0212(5)
C(m2)	0.0384(3)	−0.1143(2)	0.2401(2)	0.0207(5)
C(m3)	−0.3087(2)	0.1175(2)	0.0277(2)	0.0214(5)
C(m4)	0.0289(3)	0.3634(2)	−0.0630(2)	0.0238(5)

[a] Numbers in parentheses are the estimated standard deviations. [b] U(eq) is defined as one-third of the trace of the orthogonalized $\mathbf{U}_{ij}$ tensor.

Table 3. Bond Lengths (Å) for (Porphinato)nickel(II) [Ni(P)][a]

Ni(1)−N(1)	1.952(2)	C(a5)−C(m2)	1.370(4)
Ni(1)−N(2)	1.949(2)	C(a6)−C(m3)	1.371(4)
Ni(1)−N(3)	1.950(2)	C(a7)−C(m3)	1.373(4)
Ni(1)−N(4)	1.952(2)	C(a8)−C(m4)	1.366(4)
N(1)−C(a1)	1.376(3)	C(a1)−C(b1)	1.433(3)
N(1)−C(a2)	1.379(3)	C(a2)−C(b2)	1.434(3)
N(2)−C(a3)	1.379(3)	C(a3)−C(b3)	1.433(3)
N(2)−C(a4)	1.380(3)	C(a4)−C(b4)	1.435(3)
N(3)−C(a5)	1.379(3)	C(a5)−C(b5)	1.431(3)
N(3)−C(a6)	1.377(3)	C(a6)−C(b6)	1.440(3)
N(4)−C(a7)	1.377(3)	C(a7)−C(b7)	1.441(3)
N(4)−C(a8)	1.383(3)	C(a8)−C(b8)	1.432(4)
C(1a)−C(m4)	1.375(4)	C(b1)−C(b2)	1.343(4)
C(a2)−C(m1)	1.370(4)	C(b3)−C(b4)	1.349(4)
C(a3)−C(m1)	1.372(4)	C(b5)−C(b6)	1.347(4)
C(a4)−C(m2)	1.372(4)	C(b7)−C(b8)	1.350(4)

[a] Numbers in parentheses are the estimated standard deviations.

of the Supporting Information.) The individual bond distances and angles are given in Tables 3 and 4, respectively. A mean plane was fitted to the 24 atoms of the macrocycle defined according to Schomaker and co-workers.[39] The deviations of

(39) Schomaker, V.; Waser, J.; Marsh, R E.; Bergman, G. *Acta Crystallogr.* **1959**, *12*, 600.

Table 4. Bond Angles (deg) for (Porphinato)nickel(II) [Ni(P)][a]

N(1)−Ni(1)−N(2)	89.94(9)	N(2)−C(a4)−C(b4)	111.0(2)
N(1)−Ni(1)−N(3)	179.57(8)	N(2)−C(a4)−C(m2)	125.5(2)
N(1)−Ni(1)−N(4)	89.83(9)	C(b4)−C(a4)−C(m2)	123.5(2)
N(2)−Ni(1)−N(3)	90.00(9)	N(3)−C(a5)−C(b5)	111.1(2)
N(2)−Ni(1)−N(4)	179.07(8)	N(3)−C(a5)−C(m2)	125.3(2)
N(3)−Ni(1)−N(4)	90.22(9)	C(b5)−C(a5)−C(m2)	123.6(2)
Ni(1)−N(1)−C(a1)	127.8(2)	N(3)−C(a6)−C(b6)	110.7(2)
Ni(1)−N(1)−C(a2)	127.7(2)	N(3)−C(a6)−C(m3)	125.7(2)
C(a1)−N(1)−C(a2)	104.5(2)	C(b6)−C(a6)−C(m3)	123.6(2)
Ni(1)−N(2)−C(a3)	128.1(2)	N(4)−C(a7)−C(b7)	111.1(2)
Ni(1)−N(2)−C(a4)	127.7(2)	N(4)−C(a7)−C(m3)	125.4(2)
C(a3)−N(2)−C(a4)	104.2(2)	C(b7)−C(a7)−C(m3)	123.4(2)
Ni(1)−N(3)−C(a5)	127.9(2)	N(4)−C(a8)−C(b8)	111.3(2)
Ni(1)−N(3)−C(a6)	127.6(2)	N(4)−C(a8)−C(m4)	124.9(2)
C(a5)−N(3)−C(a6)	104.5(2)	C(b8)−C(a8)−C(m4)	123.8(2)
Ni(1)−N(4)−C(a7)	127.7(2)	C(a1)−C(b1)−C(b2)	106.6(2)
Ni(1)−N(4)−C(a8)	128.2(2)	C(a2)−C(b2)−C(b1)	107.2(2)
C(a7)−N(4)−C(a8)	104.1(2)	C(a3)−C(b3)−C(b4)	106.6(2)
N(1)−C(a1)−C(b1)	111.1(2)	C(a4)−C(b4)−C(b3)	106.9(2)
N(1)−C(a1)−C(m4)	125.5(2)	C(a5)−C(b5)−C(b6)	106.9(2)
C(b1)−C(a1)−C(m4)	123.4(2)	C(a6)−C(b6)−C(b5)	106.8(2)
N(1)−C(a2)−C(b2)	110.6(2)	C(a7)−C(b7)−C(b8)	106.6(2)
N(1)−C(a2)−C(m1)	125.6(2)	C(a8)−C(b8)−C(b7)	106.8(2)
C(b2)−C(a2)−C(m1)	123.8(2)	C(a2)−C(m1)−C(a3)	123.4(2)
N(2)−C(a3)−C(b3)	111.3(2)	C(a4)−C(m2)−C(a5)	123.4(2)
N(2)−C(a3)−C(m1)	125.2(2)	C(a6)−C(m3)−C(a7)	123.4(2)
C(b3)−C(a3)−C(m1)	123.5(2)	C(a8)−C(m4)−C(a1)	123.7(2)

[a] Numbers in parentheses are the estimated standard deviations.

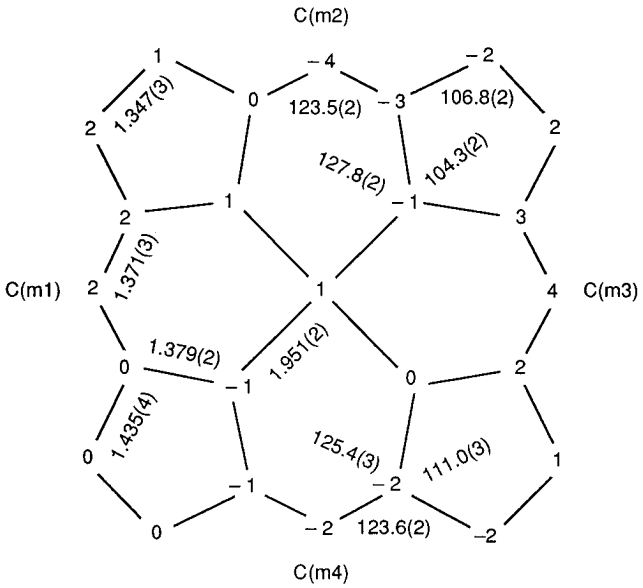

Figure 2. Formal diagram of the macrocycle of Ni(P). The out-of-plane displacements (in units of 0.01 Å) of each atom from the 24-atom mean plane are entered at the atom positions, and the average bond distances (Å) and bond angles (deg) are also shown.

the individual atoms from this mean plane and the bond distances and angles are given in Figure 2. For comparison, the average bond distances and angles as well as the root-mean-square out-of-plane displacements[40] of the planar and nonplanar crystalline forms of Ni(OEP) are summarized in Table 5. Important structural parameters are the average nickel−nitrogen

(40) The root-mean-square out-of-plane displacement Δ is defined as follows:

$$\Delta = \sqrt{\sum_{i=1}^{24} \frac{\delta_i^2}{24}}$$

δ_i is the orthogonal displacement of the macrocyclic atom i from the mean plane. The sum includes all 24 atoms of the porphyrin macrocycle.

Table 5. Selected Structural Parameters for Crystalline (Octaethylporphinato)nickel(II) [Ni(OEP)] and (Porphinato)nickel(II) [Ni(P)][a]

	Ni(OEP)			
parameter	triclinic *A*[b]	triclinic *B*[c]	tetragonal[d]	Ni(P) monoclinic[e]
NiN/Å	1.958(2)	1.952	1.929(3)	1.951(2)
$C_\beta C_\beta$/Å	1.346(2)	1.332	1.362(5)	1.347(3)
$C_\alpha C_\beta$/Å	1.443(3)	1.445	1.449(5)	1.435(4)
$C_\alpha C_m$/Å	1.371(4)	1.364	1.372(5)	1.371(3)
C_αN/Å	1.376(6)	1.386	1.387(4)	1.379(2)
NNiN[f]/deg	90.15(9)	90.1(2)	90.0	90.0(1)
$NiNC_\alpha$/deg	128.0	128.0	127.5	127.8(2)
$C_\alpha NC_\alpha$/deg	103.9(4)	103.8	105.1	104.3(2)
$NC_\alpha C_m$/deg	124.4(3)	124.4	124.0	125.4(3)
$NC_\alpha C_\beta$/deg	111.6(3)	110.8	110.7	111.0(3)
$C_\beta C_\alpha C_m$/deg	124.1(4)	124.8	125.0	123.6(2)
$C_\alpha C_m C_\alpha$/deg	125.1(1)	125.2(4)	124.1	123.5(2)
$C_\alpha C_\beta C_\beta$/deg	106.5(4)	107.2	106.9	106.8(2)
$C_\alpha NNC_\alpha$[g]/deg	0.0	0.0	32.8	1.7
rms displacement[h]/ 10^{-2} × Å	1.8	2.9	29.8	1.9
lateral shift[i]/Å	6.78	3.36	7.46	1.53
mean plane separation[i]/Å	3.48	3.45	3.46	3.36

[a] Numbers in parentheses are the estimated standard deviations. [b] Planar crystalline form.[22] [c] Planar crystalline form with geometrically nonequivalent parameters due to $\pi-\pi$ interactions; average values are shown.[23] [d] Nonplanar, ruffled form.[24] [e] Data taken from this work. [f] Adjacent nitrogen atoms. [g] Magnitude of the average torsional angle of the opposite pyrrole ring planes with respect to an axis through the nitrogen atoms. [h] Root-mean-square out-of-plane displacement from the mean plane; definition is given in ref 40. [i] Ni(OEP) data were taken from ref 19.

bond distance (NiN) and the average dihedral angle ($C_\alpha NNC_\alpha$) of opposite pyrrole planes; the values are 1.951 Å and 1.7°, respectively. The NiN distance and $C_\alpha NNC_\alpha$ angle are comparable to those values reported for planar nickel derivatives such as the planar structures of Ni(OEP) (see Table 5). A closer inspection of the out-of-plane displacement of the macrocyclic atoms indicates a very small B_{1u}-symmetry ruffling of the macrocycle.[15] (The complete crystallographic data are given in Table S2 of the Supporting Information.)

In the crystal, Ni(P) molecules form an array of laterally shifted dimers. Figure S1 in the Supporting Information shows an edge-on view of two Ni(P) molecules in the dimer configuration. The intermolecular distances are also displayed; specifically, the Ni···Ni distance is 3.716 Å, the lateral shift is 1.528 Å, and the mean plane separation is 3.355 Å. In Figure 3, a view of two Ni(P) molecules is shown in a direction perpendicular to that of Figure S1 in the Supporting Information illustrating the relative overlaps of the porphine macrocycles in this dimer configuration. Because of the small mean plane separation and lateral shift, the Ni(P) molecules are expected to interact strongly via $\pi-\pi$ interactions, consistent with the crystallographic packing arrangement of class S in the categorization of Scheidt and Lee.[19]

Spectroscopy. Figure 4 presents the Raman spectra in the 1300−1700-cm^{-1} range of Ni(P) as a single crystal and in solution (CS_2) excited with the wavelengths 413.1 and 514.5 nm. The interesting lines are labeled as $\nu_{26}(A_{2g})$, $\nu_{29}(B_{2g})$, $\nu_4(A_{1g})$, $\nu_2(A_{1g})$, $\nu_{19}(A_{2g})$, and $\nu_{10}(B_{1g})$. The assignment, symmetry, and labeling of the lines are based on the latest normal-mode analyses of Ni(P)[41] and resonance Raman excitation profile investigations.[28] The two excitation wavelengths used selectively bring out modes with the symmetry type of $A_{1g}(p)$, $A_{2g}(ap)$, $B_{1g}(dp)$, and $B_{2g}(dp)$ based on the D_{4h} point group[42b] of Ni(P) [p = polarized ($\rho \approx {}^1/_8$); ap = anomalously polarized ($\rho \approx \infty$); dp = depolarized ($\rho \approx {}^3/_4$);[43,44] the depolarization ratio $I_\perp/I_\parallel$ is designated by the symbol ρ].

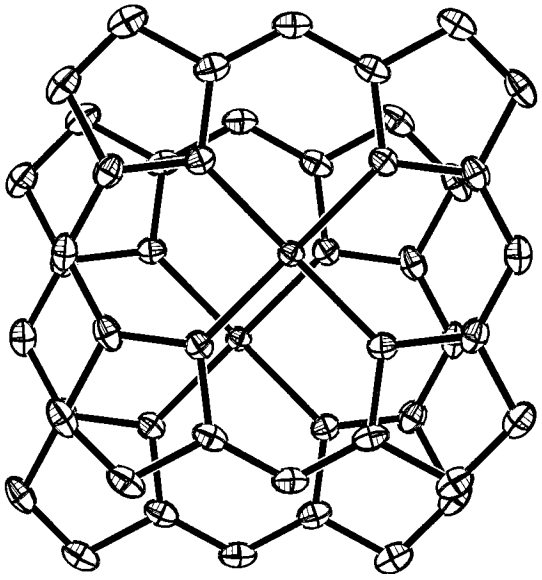

Figure 3. Overlap diagram showing the two of the interacting Ni(P) molecules. Figure S1 in the Supporting Information shows and edge-on view of these Ni(P) molecules in a direction perpendicular to this figure.

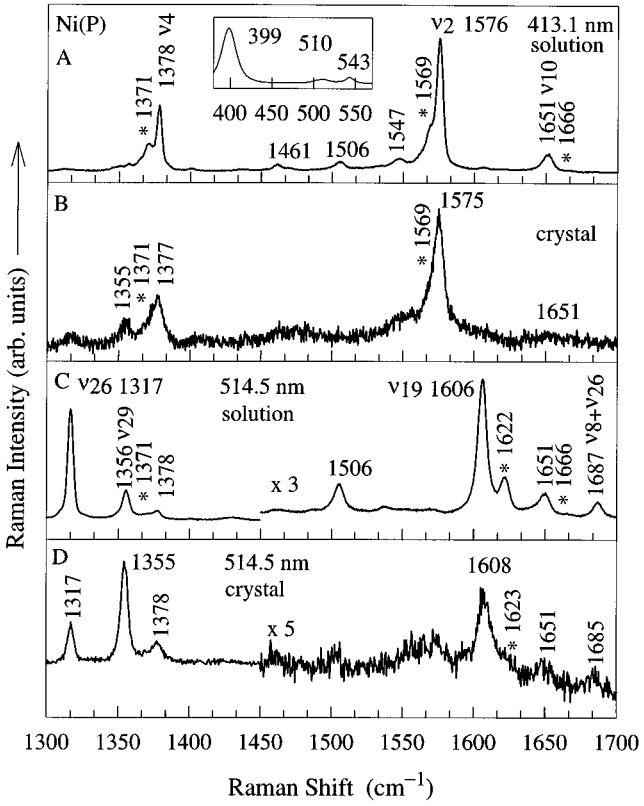

Figure 4. Resonance Raman spectra in the 1300−1700-cm^{-1} region of Ni(P) in CS_2 solution (A, C) and as a single crystal (B, D). The spectra were obtained by exciting the B and Q bands of the UV−visible spectrum (inset) to enhance different modes selectively. The sidebands are marked with asterisks (*). Typical conditions: ~150 mW (solution), 10 mW (crystal); spectral slit width for 413.1 nm (at 1500 cm^{-1}) is 2.6 cm^{-1} (solution) and 5.2 cm^{-1} (crystal), spectral slit width for 514.5 nm (at 1500 cm^{-1}) is in solution and crystal 3.2 cm^{-1}; increment 0.3 cm^{-1}/s.

(41) Li, X.-Y.; Czernuszewics, R. S.; Kincaid, J. R.; Su, Y. O.; Spiro, T. G. *J. Phys. Chem.* **1990**, *94*, 31.

Table 6. Observed Frequency Positions (cm^{-1}) of Resonance Raman Lines of (Porphinato)nickel(II) [Ni(P)] as a Single Crystal and in Solution (CS_2)

line	single crystal (C)	solution (S)	Δ(C−S)[a]
$\nu_{26}(A_2g)$	1317.4	1316.6	$+0.8 \pm 1.0$
$\nu_{29}(B_{2g})$	1354.5	1355.5	-1.0 ± 2.0
$\nu_4(A_{1g})$	1377.3	1378.0	-0.7 ± 1.0
$\nu_2(A_{1g})$	1575.2	1575.7	-0.5 ± 1.0
$\nu_{19}(A_{2g})$	1608.0	1606.0	$+2.0 \pm 1.0$
$\nu_{10}(B_{1g})$	1651.0	1651.1	-0.1 ± 2.0

[a] Frequency differences (cm^{-1}) between single crystal (C) and solution (S) along with their estimated errors.

The different enhancement patterns of the lines are well understood.[28,45] The A_{1g} modes are dominant in the vicinity of the strong B band (Franck−Condon scattering). The B_{1g} and B_{2g} modes are enhanced in the Q-band excitation via interstate (Herzberg−Teller scattering) and intrastate vibronic coupling (Jahn−Teller scattering); the appearance of B-band excited B_{1g} and B_{2g} modes is a result of Jahn−Teller coupling between the degenerate components of the electronic B states.[45] The A_{2g} modes are symmetry forbidden in normal Raman scattering, but they appear in resonance Raman scattering through interstate vibronic coupling with the B states under Q-band excitation.

It is well-known that the frequency positions of the in-plane skeletal modes in the 1300−1700-cm^{-1} range are sensitive to the oxidation state (or electron density) of the central metal,[42a,b] the core size,[14,15,42d−f] nonplanarity of the macrocycle,[14,15,25,42g] and axial ligands.[42c] Some structure-sensitive lines are shown in Figure 4 and are usually designated as oxidation-state (ν_4) and core-size marker lines (ν_2, ν_{19}, ν_{10}).

Table 6 lists the observed frequency positions of the structure-sensitive lines of Ni(P) as a single crystal and in solution and their frequency differences between single crystal and solution. As can be seen from Table 6, no significant differences in frequency are noted for the structure-sensitive lines ν_2, ν_{10} or the lines ν_{26}, ν_{29}. Only the structure-sensitive line ν_{19} shows a significant upshift of 2 ± 1 cm^{-1} with respect to the solution data.

It was previously reported that the solution Raman spectra of Ni(P) show a sideband for each of the structure-sensitive lines ν_4, ν_2, ν_{19}, and ν_{10}.[28,29] This observation was interpreted in terms of an equilibrium between two conformers. Figure 5 (upper panel) shows an enlarged view of the lines ν_4, ν_2, and ν_{19} from Ni(P) in solution. The most intensive lines appear at 1378, 1576, and 1606 cm^{-1}, and the corresponding weak sidebands (marked with asterisks), at 1371, 1569, and 1622 cm^{-1}, respectively. The very weak sideband of ν_{10} is at 1666 cm^{-1} (not shown Figure 5); its position in solution was taken from an earlier study.[29] The Raman spectra of the single crystal from which we obtained the X-ray crystal structure are also shown in Figure 5 (lower panel). It is obvious that the sidebands of ν_4, ν_2, and ν_{19} are also present in the single-crystal spectra.

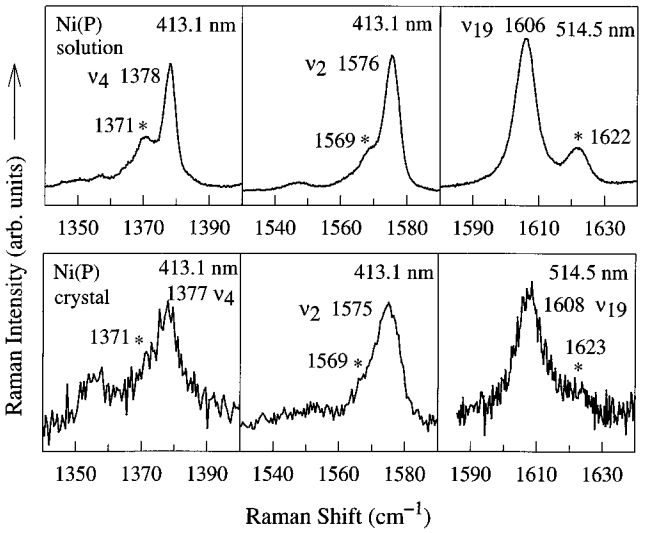

Figure 5. Enlarged view of the resonance Raman lines ν_4, ν_2, and ν_{19} of Ni(P) in CS_2 solution (upper panels) and as a single crystal (lower panels). The sidebands are marked with asterisks (*). The experimental conditions are the same as in Figure 4.

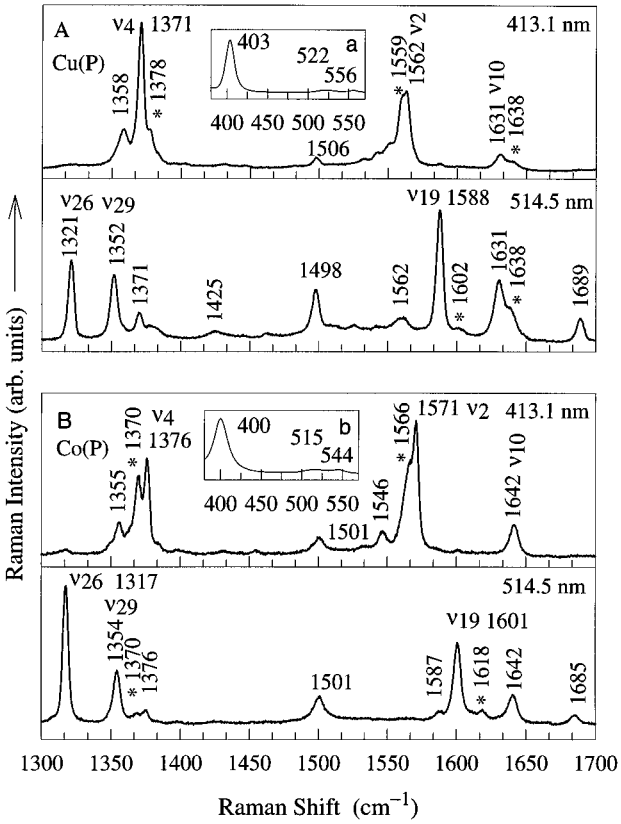

Figure 6. Resonance Raman spectra in the 1300−1700-cm^{-1} region of Cu(P) (A) and Co(P) (B) in CS_2 solution. The spectra were obtained by exciting the B and Q bands of the UV−visible spectrum (insets a, b) to enhance different modes selectively. The sidebands are marked with asterisks (*). Typical conditions: ~150 mW; spectral slit width at 1500 cm^{-1} is 2.6 cm^{-1} (413.1 nm) and 3.2 cm^{-1} (514.5 nm); increment 0.3 cm^{-1}/s.

Furthermore, the sidebands also occur for other metal derivatives investigated; the Raman spectra of Cu(P) and Co(P) in CS_2 solution are shown in Figure 6. The assignment of the lines and their sidebands for these metalloporphines is made by using Ni(P) as reference and by measurements of the depolarization ratios. It is interesting to note that line ν_{10} of Cu(P) clearly exhibits an intensive high-frequency shoulder which is less prominent in the spectra of Ni(P). Verma and

(42) (a) Yamamoto, T.; Palmer, G.; Gill, D.; Salmeen, I. T.; Rimai, L. *J. Biol. Chem.* **1973**, *248*, 5211. (b) Spiro, T. G.; Strekas, T. C. *J. Am. Chem. Soc.* **1974**, *96*, 338. (c) Kitagawa, T.; Ogoshi, H.; Watanabe, E.; Yoshida, Z. *J. Phys. Chem.* **1975**, *79*, 2629. (d) Spaulding, L. D.; Chang, C. C.; Yu, N.-T.; Felton, R. H. *J. Am. Chem. Soc.* **1975**, *97*, 2517. (e) Stong, J. D.; Spiro, T. G.; Kubaska, R. J.; Shupack, S. I. *J. Raman Spectrosc.* **1980**, *9*, 312. (f) Parthasrathi, N.; Hansen, C.; Yamaguchi, S.; Spiro, T. G. *J. Am. Chem. Soc.* **1987**, *109*, 3865. (g) Prendergast, K.; Spiro, T. G. *J. Am. Chem. Soc.* **1992**, *114*, 3793.
(43) Verma, A. L.; Bernstein, H. J. *J. Chem. Phys.* **1974**, *61*, 2560.
(44) (a) McClain, W. M. *J. Chem. Phys.* **1971**, *55*, 2789. (b) Zgierski, M. Z.; Pawlikowski, M. *J. Chem. Phys.* **1982**, *65*, 335.
(45) (a) Shelnutt, J. A.; Cheung, L. D.; Chang, R. C. C.; Yu, N.-T.; Felton, R. H. *J. Chem. Phys.* **1977**, *66*, 3387. (b) Shelnutt, J. A.; O'Shea, D. C. *J. Chem. Phys.* **1978**, *69*, 5361. (c) Shelnutt, J. A. *J. Chem. Phys.* **1980**, *72*, 3948. (d) Shelnutt, J. A. *J. Chem. Phys.* **1981**, *74*, 6644.

co-workers[43,46] also noticed the sideband of ν_{10} for Cu(P) and the sideband of ν_{19} for Ni(P). The origin of these doublets is a phenomenon that will be discussed in the next section.

In contrast to many substituted metalloporphyrins, the metalloporphines generally have poor solubility in most solvents. Although not likely, it is possible that metalloporphines in solution exist as monomers and dimers or even higher aggregates which could be associated with the appearance of the sidebands in the Raman spectra. To investigate this possibility, the concentration of Ni(P) was systematically decreased to about 1 μM, and the corresponding UV−visible absorption and Raman spectra were recorded. The inset of Figure 4 shows the UV−visible absorption spectrum of Ni(P) containing the strong B and the weak Q band. No changes in the shape of the UV−visible absorption spectra and Raman spectra were observed upon dilution, indicating that aggregations are probably not associated with the appearance of the sidebands in the Raman spectra (*vide infra*).

Discussion

Crystal Structure. From Figures 1 and 2, it can clearly be seen that Ni(P) is nearly planar in the solid state. Both the root-mean-square out-of-plane displacement[40] of the 24-atom macrocycle (0.019 Å) and the average dihedral angle $C_\alpha NNC_\alpha$ (1.7°) of the opposite pyrrole ring planes are relatively small.

The average nickel−nitrogen distance of 1.951 Å for Ni(P) is slightly smaller than the typical 1.96 Å value for nickel derivatives with planar macrocycles,[22,47] but it is within the range of values observed for nickel−porphyrin X-ray structures. For example, the nickel−nitrogen distance agress well with the average value of 1.952 Å of the planar triclinic *B* form of Ni(OEP) which is also found in a packing arrangement with a small lateral shift.[23] Also of note are the unchanged $C_\beta C_\beta$ bond distances from Ni(P) to the planar structures of Ni(OEP). This implies that the repulsion of the two ethyl groups bonded at the same pyrrole ring does not directly influence the geometry of the pyrrole rings. Taken together, the structural parameters of Ni(P) in the crystal do not show remarkable deviations from those of other planar nickel porphyrins [*e.g.*, Ni(OEP) (see Table 5)].

The crystal packing arrangement of Ni(P) shown in Figure 3 and Figure S1 in the Supporting Information demonstrates the close stacking configuration of the Ni(P) dimer. The dimer geometry is characterized by a small intermolecular separation of 3.355 Å and a lateral shift of 1.528 Å. Analogously packed dimer configurations in the solid state are observed in five-coordinated nitrosyl(octaethylporphinato)iron(III),[48a] $[Fe(OEP)(NO)]^+$, and (2-methylimidazole)(octaethylporphinato)iron(III),[48b] $[Fe(OEP)(2\text{-MeHIm})]^+$, in which the two iron(III) ions communicate via $\pi-\pi$ interactions.[49]

Accordingly, the strong overlap between the porphinato macrocycles of the Ni(P) dimer is thought to cause an asymmetric, strong $\pi-\pi$ interaction field resulting in asymmetric structural parameters.[23,50,51] For example, the crystal stacking arrangement of Ni(OEP) in the triclinic *B* form gives an intermolecular separation of 3.45 Å and a lateral shift of 3.36 Å and clearly exhibits smaller metal−nitrogen distances [1.946(4) versus 1.958(4) Å] and $C_\alpha NC_\alpha$ angles [103.5(4) versus 104.6(4)°] for those pyrroles which are positioned favorably for $\pi-\pi$ interactions.[23] Ibers and co-workers[51] have also observed a similar stacking arrangement in Ni(TMeP) [(*meso*-tetramethylporphinato)nickel(II)]. However, for Ni(TMeP), theoretical calculations and an experimental bonding electron density study were not able to interpret the observed nonequivalent geometrical changes solely by a charge density shift.

These asymmetric changes are not observed for Ni(P). In fact, the strong $\pi-\pi$ interaction field is not reflected in differences in the geometrical parameters of the Ni(P) dimer. In addition, the $\pi-\pi$ interaction in the Ni(P) dimer configuration is expected to be even larger than that for the triclinic *B* form of Ni(OEP) on the basis of the intermolecular separations and the lateral shifts as a measure for the $\pi-\pi$ interactions. This finding is consistent with the above mentioned tightly packed $[Fe(OEP)(NO)]^+$ and $[Fe(OEP)(2\text{-MeHIm})]^+$ dimers, in which the equivalent bond distances and angles are also similar.

In conclusion, the occurrence of geometrically nonequivalent parameters in a stacking arrangement may be indicative of a $\pi-\pi$ interaction, but the presence of a strong $\pi-\pi$ interaction field does not necessarily cause differences in geometrically equivalent parameters. A possible explanation for the absence of nonequivalent parameters for the Ni(P) dimer configuration could be the small lateral shift resulting in a more symmetric field for the $\pi-\pi$ interactions than that in the triclinic *B* form of Ni(OEP).

Resonance Raman Spectroscopy and Structure in Solution. The frequency positions of the structure-sensitive Raman lines in the 1300−1700-cm^{-1} range are known to be sensitive to different crystal packing arrangements[23,49] and aggregation in solution.[7,27] For example, both Ni(OEP)[22,23] and Cu(OEP)[21b] crystallize in both the triclinic *A* and *B* forms, and the *B* forms show stronger $\pi-\pi$ interactions than the *A* forms, resulting in frequency shifts of several structure-sensitive Raman lines between triclinic *A* and *B*. These different crystal packing arrangements generally cause an average upshift on the order of 3 cm^{-1} for lines ν_4, ν_2, ν_{19}, and ν_{10} with respect to those crystalline forms in which the $\pi-\pi$ interactions are weak.[21b,23] Furthermore, these shifts are similar to those observed in solution studies of $\pi-\pi$ aggregation.[7,27] In the Ni(P) case, we do not have both "dimer crystals" and "monomer crystals" to compare. Nevertheless, it is interesting to compare the frequency positions of the structure-sensitive Raman lines of Ni(P) in solution (monomer) with the frequencies in the crystal (dimer) in order to obtain related information about the structural changes caused by $\pi-\pi$ interactions in the crystal.

Figure 4 displays the Raman spectra, and Table 6 summarizes the observed frequency positions and their shifts from solid state to solution. Except for line ν_{19}, no significant frequency shifts are observed. Line ν_{19} exhibits an upshift of about 2.0 ± 1 cm^{-1}, possibly indicating a weak $\pi-\pi$ interaction. However, because the frequency positions in solid state and solution generally deviate by approximately ± 2 cm^{-1},[36,52] the $\pi-\pi$ interactions in the crystal cannot be corroborated by Raman spectroscopy.

(46) Verma, A. L.; Asselin, M.; Sunder, S.; Bernstein, H. J. *J. Raman Spectrosc.* **1976**, *4*, 295.
(47) (a) Hoard, J. L. *Ann. N.Y. Acad. Sci.* **1973**, *206*, 18. (b) Hamor, T. A.; Caughey, W. S.; Hoard, J. L. *J. Am. Chem. Soc.* **1965**, *87*, 2305.
(48) (a) Scheidt, W. R.; Lee, Y. J.; Hatano, K. *J. Am. Chem. Soc.* **1984**, *106*, 3191. (b) Scheidt, W. R.; Geiger, D. K.; Lee, Y. J.; Reed, C. *J. Am. Chem. Soc.* **1985**, *107*, 5693.
(49) Gupta, G. P.; Lang, G.; Scheidt, W. R.; Geiger, D. G.; Reed, C. A. *J. Phys. Chem.* **1983**, *11*, 5945.
(50) (a) Gallucci, J. C.; Sweptson, P. N.; Ibers, J. A. *Acta Crystallogr., Sect. B* **1982**, *38*, 2134. (b) Straus, S. H.; Silver, M. E.; Long, K. M.; Thompson, R. G.; Hudgens, R. A.; Spartalian, K.; Ibers, J. A. *J. Am. Chem. Soc.* **1985** *107*, 4207.
(51) Kutzler, F. W.; Sweptson, P. N.; Berkovitch-Yellin, Z.; Ellis, D. E.; Ibers, J. A. *J. Am. Chem. Soc.* **1983**, *105*, 2996.
(52) According to a recent investigation of nickel(II) *meso*-tetrasubstituted porphyrins,[15] the frequency differences of the structure-sensitive Raman lines between solid state and solution (CS_2) deviate only ± 2 cm^{-1}, assuming that no structural changes from solution to solid state occur and the solvent−solute interactions are weak. Jentzen, W.; Shelnutt, J. A. Unpublished results.

A remarkable feature of the Raman spectra of Ni(P) in solution is the sidebands observed for some structure-sensitive lines such as ν_4, ν_2, and ν_{19} (see Figure 5). It was previously demonstrated that, except for a scaling factor, each line and its sideband exhibit almost the same shape for their resonance Raman excitation profiles.[28] Additionally, each pair has the same depolarization ratio over the 420−500-nm excitation range,[28] and Raman measurements at temperatures between 200 and 330 K reveal that the intensity ratios of the line and its sidebands are also temperature-independent.[29] Together, the similar behavior for each line and its sideband suggests a similar origin for the two lines, possibly the same vibrational mode arising from the molecule existing as different conformers or in different environments.

At first, the poor solubility of all metalloporphines suggests that dimerization (or even higher aggregation) in solution might be associated with the appearance of additional Raman lines. That is, the presence of both monomer and aggregate might account for the two forms. This possibility was checked by recording the UV−visible absorption and Raman spectra at different porphine concentrations.[7,27] However, the UV−visible absorption and Raman spectra of Ni(P) are independent of concentration; thus aggregation in solution is probably not associated with the appearance of the sidebands. In any case, aggregation would not be expected to give the large shifts in frequencies.

A more appealing suggestion was that Ni(P) might exist in solution as two conformers with almost equal Gibbs energies.[28,29] The lines and their sidebands were therefore assigned to planar and nonplanar conformers in analogy with Ni(OEP),[26] even though the sidebands appear on the wrong side of the lines in a few cases. However, the appearance of the sidebands in the single-crystal Raman spectra of Ni(P) negates this interpretation. Because the crystal contains only the planar conformer, the single-crystal Raman spectra are expected to reveal only single lines for ν_4, ν_2, and ν_{19}. As can be seen from Figure 5, the sidebands clearly remain in the single-crystal Raman spectra. In addition, the sidebands appear even for other metalloporphines investigated, namely Cu(P) and Co(P) (see Figure 6), which are expected to exist in only the planar conformation in solution, since these central metals give core sizes closer to the optimum porphyrin core size. [The sidebands in the spectra of Cu(P) and Co(P) are also marked with asterisks.]

Hence, the similarities of the single-crytal and solution Raman spectra of Ni(P) as well as the fact that the sidebands also appear in the solution Raman spectra of Cu(P) and Co(P) strongly suggest that Ni(P) in solution exists only as the planar structure rather than in an equilibrium between two conformers. We must therefore search for an alternative assignment for the sidebands. Raman spectra of deuterated Ni(P) [*meso*-d_4, pyrrole-d_4, and (*meso* and pyrrole)-d_{12} isotopomers] support this conclusion because the appearance of the sidebands depends on isotopic substitution (see Figures 5 and 6 in the work of Li and co-workers[41]). This is indeed unexpected if the lines and sidebands were due to a conformational equilibrium.

Origin of the Sidebands. The occurrence of the sidebands for Ni(P), Cu(P), and Co(P) is a phenomenon that is not resolved completely, but we surmise that the sidebands are binary overtone or combination lines. These lines appear because of the strong anharmonicity present in metalloporphyrins.[53] Possible assignments for the nonfundamental lines for Ni(P) which satisfy both the frequency positions and the symmetry properties of the sidebands are listed in Table 7. One potential problem with these assignments is accounting for the strong enhancement of the sidebands in the B-band-excited Raman spectra. Because the line and its sidebands have the same symmetry, Fermi resonance interaction between them might be operative. As a consequence, the sidebands are significantly stronger than the observed high-frequency nonfundamentals in the 2000−4000-cm^{-1} region which were obtained under B-band excitation (data not shown). Moreover, Fermi resonance also accounts for the very weak intensity of the sideband of ν_{10} for Ni(P) compared to the sidebands of ν_4, ν_2, and ν_{19} (see Table 7) because the calculated symmetry of the combination line (sideband) of ν_{10} is different from the fundamental line.

Table 7. Tentative Assignment of the Raman Sidebands of (Porphinato)nickel(II) [Ni(P)] to Nonfundamental Lines (Combination Lines)

assignment[a]	obsd[b]	calcd[c]	I_{main}/I_{side}[d]
$\nu_8(A_{1g}) + \nu_6(A_{1g})$	1371 (A_{1g})	1364 (A_{1g})	≈3
$\nu_{21}(A_{2g}) + \nu_{25}(A_{2g})$	1569 (A_{1g})	1568 (A_{1g})	≈4
$\nu_{13}(B_{1g}) + \nu_{33}(B_{2g})$	1622 (A_{2g})	1620 (A_{2g})	≈3
$\nu_3(A_{1g}) + \nu_{35}(B_{2g})$	1666 (B_{1g}/B_{2g})[e]	1656 (B_{2g})	≈9[e]

[a] Frequency positions of the fundamentals were taken from Li and co-workers.[41] [b] Frequency position (cm^{-1}). [c] Calculated frequency positions (cm^{-1}) are based on the observed fundamental frequencies. [d] Intensity ratio of the main line (fundamental) and its sideband (nonfundamental). Intensity is defined as the area of the line. [e] Data were taken from ref 29; accuracy in the frequency position is ±2 cm^{-1}.

The most vexing problem with respect to the assignment of these lines as nonfundamentals is that the resonance Raman excitation profiles of the fundamental lines and nonfundamental sidebands are similar. As mentioned previously, each pair exhibits the same shape for their resonance Raman excitation profiles in the Q-band region. In other words, the profiles of the sidebands have almost the same peak positions at both 0−1 and 0−0 resonances as the corresponding fundamental lines, and the 0−1 and 0−0 intensity ratios are also similar. Because of the different scattering mechanisms that contribute to the resonance Raman enhancements for fundamentals and combinations (or overtones), it would be expected that the resonance Raman excitation profiles would be different.[54] On the other hand, the experimentally measured excitation profiles for two known combination lines[41,55] $\nu_8(A_{1g}) + \nu_{24}(A_{2g})$[55a] and $\nu_8(A_{1g}) + \nu_{26}(A_{2g})$[55b] at 1175 and 1687 cm^{-1}, respectively, surprisingly show the same features as A_{2g} fundamentals. Accordingly, it is conceivable that the observed sidebands in the Raman spectra of metalloporphines investigated are due to nonfundamentals. The theoretical explanation of the resonance Raman excitation profiles for fundamentals, overtones, and combinations as well as the effect of Fermi resonance interaction on the excitation profile will be addressed in a future paper.

Conclusions

The crystal structure and the single-crystal and solution Raman spectra provide useful information about interaction in the crystal and the structure in solution. Two paramount conclusions can be drawn from this investigation. First,

(53) (a) Asher, S. A.; Murtaugh, J. *J. Am. Chem. Soc.* **1983**, *105*, 7244. (b) Schweitzer-Stenner, R.; Jentzen, W.; Dreybrodt, W. In *Proceedings of the Fifth International Conference on the Spectroscopy of Biological Systems*; Theophanides, T., Anastassopoulou, J., Fotopoulos, N., Eds.; Kluwer Academic Publishers: Dordrecht, The Netherlands, 1993; p 31.

(54) (a) Friedman, J. M.; Hochstrasser, R. M. *Chem. Phys.* **1973**, *1*, 457. (b) Friedman, J. M.; Hochstrasser, R. M. *J. Am. Chem. Soc.* **1976**, *98*, 4043. (c) Gladkov, L. L.; Gradyushko, A.; Ksenofontova, N. M.; Solovyov, K. N.; Starukhin, A. S.; Shulga, A. M. *J. Appl. Spectrosc.* **1978**, *28*, 462. (d) Aramaki, S.; Hamaguchi, H.; Tasumi, M. *Chem. Phys. Lett.* **1983**, *96*, 555.

(55) (a) Unger, E. Diploma Thesis, University of Bremen, Germany, May 1992. (b) Unger, E. Personal communication.

although a strong $\pi-\pi$ interaction in the tightly packed dimer configuration can be inferred from the small interplanar separation, it could not be positively confirmed by comparison of the single-crystal and solution Raman spectra which reveals small and unsystematic frequency differences. Second, Ni(P) is the least sterically crowded nickel porphyrin in terms of peripheral substituents, and it is planar as a single crystal and in solution. While this might seem to be an obvious conclusion, other nickel porphyrins with only slightly more crowded substituents than Ni(P) do frequently exist in at least two conformations in solution. For example, by using X-ray diffraction and Raman spectroscopy, we recently showed that planar and nonplanar structures coexist in solution for Ni(OEP),[26] Ni(TPP) [nickel(II) *meso*-tetraphenylporphine],[56] Ni(UroP^{8-}) [nickel(II) uroporphyrin I],[7] and Ni(ProtoP^{2-}) [nickel(II) protoporphyrin IX].[7] Consequently, substituents larger than hydrogens are required to shift energetically the conformational equilibrium toward the nonplanar structure. Thus, nickel porphyrins are poised such that only a slight increase in steric crowding at the porphyrin periphery may induce nonplanar conformations.

Acknowledgment. We thank Michele Berkey for reading the manuscript and her valuable discussions. This work was supported by U.S. Department of Energy Contract DE-AC04-94DP85000 (J.A.S.), an Associated Western Universities Postdoctoral Fellowship (W.J.), and National Institutes of Health Grants GM-38401 and RR-06709 (W.R.S.).

Supporting Information Available: Table S1, giving the fractional atomic coordinates of the hydrogen atoms, Table S2, listing complete crystallographic data, and Figure S1, showing an edge-on view of two Ni(P) molecules in the dimer configuration in a direction perpendicular to Figure 3 (4 pages). Ordering information is given on any current masthead page.

IC960157L

(56) (a) Jentzen, W.; Unger, E.; Schweitzer-Stenner, R.; Dreybrodt, W.; Subbarao, S. K.; Mahmud, T.; Hobbs, J D.; Shelnutt, J. A. *Biophys. J.* **1995**, *68*, A82. (b) Jentzen, W.; Mahmud, T.; Unger, E.; Schweitzer-Stenner, R.; Dreybrodt, W.; Turowska-Tyrk, I.; Scheidt, W. R.; Shelnutt, J. A. Abstracts of Papers, 210th National Meeting of the Chemical Society, Chicago, IL; American Chemical Society: Washington, D.C., 1995; INORG 628. (c) Jentzen, W.; Unger, E.; Turowska-Tyrk, I.; Song, X.; Nurco, D. J.; Medforth, C.J.; Smith, K. M.; Dreybrodt, W.; Schweitzer-Stenner, R.; Scheidt, W. R.; Shelnutt, J. A. In preparation.